Effect of Multiple Extrusions on the Impact Properties of Polypropylene/Clay Nanocomposites

R. Klitkou, E. A. Jensen, J. de C. Christiansen

Department of Mechanical and Manufacturing Engineering, Aalborg University, Fibigerstraede 16, Aalborg 9220, Denmark

Received 9 August 2011; accepted 6 December 2011
DOI 10.1002/app.36639
Published online in Wiley Online Library (wileyonlinelibrary.com).

ABSTRACT: Polypropylene (PP)-based polymer nanocomposites containing organically modified montmorillonite (OMMT) with and without maleic anhydride grafted PP, were compounded by twin-screw extrusion. The extrusion process was repeated various numbers of times to increase the extruder residence time (T_R) and, through that, the particle dispersion. Rheological measurements fitted to a modified Carreau–Yasuda model defining a melt yield stress were used to indicate changes in the particle dispersion with regard to T_R. This analysis showed a monotonically increased dispersion of clay particles in the PP matrix with increasing extruder T_R. The small-strain tensile properties were tested at both ambient (20°C) and elevated (90°C) temperatures, and no significant changes were observed in the tensile strength or modulus as a function of T_R. Instrumented Izod impact tests showed that the nanocomposite impact strength (σ_i) increased monotonically with increased T_R by 70% from least dispersed to best dispersed, which was still 20% below the level for neat PP. Both the fracture initiation energy and propagation energy increased with T_R, but the primary effect on σ_i came from the fracture propagation energy, which delivered 80% of the improvement. © 2012 Wiley Periodicals, Inc. J Appl Polym Sci 000: 000–000, 2012

Key words: clay; extrusion; impact resistance; nanocomposites; poly(propylene); (PP)

INTRODUCTION

The improvement of the mechanical response of polyolefin polymers by the addition of inorganic nanoclay particles and the formation of nanocomposites is an area of high academic focus because of the potential industrial impact of obtaining high-performance materials based on cheap commodity polymers. In addition to the mechanical response, active research includes permeability, flammability, and thermal stability.[1–3] The reported improvements in the mechanical response have primarily focused on increased strength and stiffness in the ranges of 5–25 and 5–50%, respectively, whereas the corresponding impact properties have been less consistent, ranging from a decrease of 30% to an increase of 100%.[4–7] In industrial applications, polymer impact properties are a very important parameter, and tailoring composite mechanical responses with the use of nanoparticles should be done with this in mind. It is well known that the addition of larger glass and carbon fibers decreases the composite toughness but significantly increases the strength and stiffness. One of the possible benefits of polymeric nanocomposites, when controlled and understood, is improved strength and stiffness with a simultaneously maintained polymer impact strength (σ_i); therefore, this is becoming an attractive alternative to conventional microcomposites.

As shown in the review by Chen and Evans,[8] significantly different results of polymer impact properties have been reported for different systems, including polyolefin–clay nanocomposites. The differences have been explained by both various test conditions and a number of different mechanisms defining the σ_i values of the clay-filled nanocomposites. Some of the reported mechanisms that have determined polyolefin–clay nanocomposite σ_i values have included the spherulite size, particle–matrix interaction and dispersion,[4] and void formation around clay fillers absorbing energy during impact.[9]

In this study, we investigated the effect of the particle dispersion on the Izod impact properties of unnotched polypropylene (PP) clay nanocomposites by applying instrumented impact equipment to analyze the development of the impact response from initial crack initiation through crack propagation and, finally, breakage of the sample.

It is generally known that the state of dispersion for clay-filled polymers ranges from fully exfoliated to a microreinforced composite containing only

Correspondence to: R. Klitkou (klitkou@m-tech.aau.dk).
Contract grant sponsor: European Commission; contract grant number: Project Nanotough-213436.
Contract grant sponsor: Danish Agency for Science Innovation and Technology through the Project Extreme Materials for Extreme Environments.

larger aggregates. Most nanocomposites will exhibit a dispersion state between these two containing aggregates, intercalated stacks, and individual exfoliated clay platelets. To draw advantages from the large surface area of the clay, some degree of separation of the platelets needs to be in place. For polyolefin systems, this is typically achieved by (1) organic modification of the clay to increase the interlayer distance and make it miscible with the organic matrix, (2) application of a compatibilizing agent capable of diffusing into the interlayer gallery, and (3) optimization of the melt-mixing procedure. Melt mixing by twin-screw extrusion (TSE) has become the preferred technique for dispersing nanoclays into the polyolefin matrix, and a substantial amount of work has been performed on the optimization of this mixing process with respect to screw profiles, extruder residence time (T_R), and specific energy (E_S) input to the material.[10–13]

We used the experience from these processing optimizations and documented changes in dispersion in this work to obtain different dispersion states for the same material composition by subjecting the materials to multiple extrusion cycles and, thereby, increasing T_R and E_S input. By obtaining different dispersion states in the same material system, we could investigate the influence on the impact properties and small-strain tensile properties at low deformation rates with regard to particle dispersion.

We evaluated the dispersion by fitting data measurements obtained by small-strain oscillatory rheological measurements to a modified Carreau–Yasuda model, including melt yield stress, as proposed by Lertwimolnun and Vergnes,[10] which also demonstrated that the melt yield stress was directly related to the degree of exfoliation. The rheological measurements were further used to monitor the matrix degradation occurring during multiple extrusion cycles. The small-tensile-strain mechanical properties were determined to evaluate the reinforcing effect of the nanofiller under the different processing conditions. Additionally, differential scanning calorimetry (DSC) was performed to evaluate any changes in the matrix crystallinity.

EXPERIMENTAL

Materials

Two PP-based polymer nanocomposites (PNCs) filled with OMMT were investigated in this work, one with a PP-*g*-maleic anhydride (MA) compatibilizer and one without. The compatibilizer was added to the system with a twofold purpose: (1) to enhance the load transfer from the matrix to the filler and (2) to help separate the individual clay platelets, that is, to increase the exfoliation of the clay. Besides the PNCs, two reference materials were subjected to similar processing conditions; one was neat PP, and the other was PP combined with PP-*g*-MA to monitor the material degradation that occurred during repeated extrusion.

TABLE I
Material Composition

Sample ID	PP (wt %)	OMMT (wt %)	PP-*g*-MA (wt %)	*n*
100/0/0–*n*	100	0	0	*n* (0, 1, 2, 3, 5)
96/4/0–*n*	96	4	0	*n* (1, 2, 3, 5)
96/0/2–*n*	98	0	2	*n* (1, 2, 3, 5)
94/4/2–*n*	94	4	2	*n* (1, 2, 3, 5)

n = number of extrusion cycles.

The matrix polymer was an isotactic PP homopolymer [Moplen HP400R, LyondellBasell, Rotterdam, Netherlands, density = 0.900 g/cm^3, melt flow rate = 25 g/10 min, melting temperature (T_m) = 160–163°C, weight-average molecular weight (M_w) = 305 kg/mol]. The compatibilizer was a PP-*g*-MA G-3015 from Eastman Chemical Co. (density = 0.913 g/cm^3, T_m = 156°C, M_w = 47 kg/mol). The OMMT was Dellite 67G from Laviosa Chimica Mineraria S. p. A. The montmorillonite was modified with dimethyl dihydrogenated tallow ammonium chloride corresponding to approximately 40 wt % according to thermogravimetry. The composition and sample ID for the used composites and reference materials are listed in Table I.

Table I shows the number of repeated extrusion cycles to which the material was subjected, where zero means no extrusion, which was only possible for neat PP.

Preparation

The PNCs and reference blends were prepared by a compounding procedure that consisted of melt blending on a TSE equipment, which led to the extrusion of a thin string, which was then continuously cooled in a bath with distilled water at ambient temperature and finally pelletized by a rotating knife. A setup from Thermo Scientific, Waltham, Massachusetts was used, which consisted of a PRISM Eurolab 16 TSE equipment with an automatic granule feeder, six temperature-controlled barrel zones, a stainless steel water bath, and an L-002-1345 pellet cutter. In Table II, the compounding parameters for one extrusion cycle are summarized.

The parameters listed in Table II are a combination of fixed equipment parameters and the resulting parameters. The fixed equipment parameters included the length-to-diameter (L/D) ratio, barrel temperature, feed rate (Q), and screw speed (N) and, together with the screw profile, determined the resulting parameters defining the mixing characteristics to which the

TABLE II
Extrusion Parameters

Parameter	Value
Barrel L/D	25
Barrel temperature, zone 1–5	200°C
Q	2.7 kg/h
N	300 rpm
Average screw torque	5.6 N m
P_{AVG}	1.18 kW
Average die pressure	6–7 bar
T_R per extrusion cycle	30 s
E_S per extrusion cycle	1570 kJ/kg

materials were subjected. Several aspects had to be considered when we set the temperature. First, the viscosity changed with temperature and, therefore, changed the specific mixing energy, but it also varied the chain mobility, which could be important for the proper dispersion of the clay platelets in the matrix.[13] Finally, excessive thermal degradation was to be avoided. In ref. 11, it was suggested that the N/Q ratio should be maximized to improve exfoliation, explained by increased T_R and E_S. These were the primary design considerations used in the setup of the compounding procedure and led to a 30-s T_R and an E_S of 1570 kJ/kg per compounding cycle. T_R was defined as the mean of the T_R distribution, and E_S was defined with eq. (1):

$$E_S = \frac{P_{AVG} \times 3600}{Q} \quad (1)$$

where P_{AVG} is the average screw power. The applied screw type was an intermeshing corotating type, and the design of the screw profile can be seen in Figure 1.

The screw configuration was a combination of forward-feeding elements and mixing elements. The forward-feeding elements had the function of transporting the material forward and building up the die pressure, together with performing distributive mixing. The mixing elements were included to increase the dispersive mixing capability and enhance the ability to break up agglomerates and separate the individual layers.

TABLE III
Injection-Molding Parameters

Parameter	Value
Barrel temperatures	220, 200, 200, 200, 200, and 45°C
Mold temperature	60°C
Cooling time	20 s
Specimen type	ISO 3167 multipurpose specimen

The injection molding of multipurpose test specimens was performed on an industrial-sized Ferromatik Milacron, Malterdingen, Germany K110 injection-molding machine with the parameters summarized in Table III.

Characterization

DSC

The thermal characterization of the materials was done by DSC with a Netzsch, Selb, Germany STA 449 C Jupiter instrument. The materials were placed in AlO_2 pans and tested in an argon atmosphere with a heating/cooling rate of 10 K/min. The test material was cut from the center of the injection-molded tensile bars in an amount of approximately 5 mg. The parameters obtained from the DSC results were (1) T_m, defined as the minimum value of the endothermic peak observed during heating; (2) crystallization temperature (T_c), defined as the maximum value of the exothermic peak during cooling; and (3) degree of crystallinity (χ_C), as defined by eq. (2):

$$\chi_C = \frac{\Delta H_m}{\Delta H_m{}^0} \times 100 \quad (2)$$

where ΔH_m is the heat of fusion observed during heating as the area of the endothermic peak and $\Delta H_m{}^0$ is the theoretical heat of fusion for a 100% crystalline PP and corresponded to 207 J/g.[14] All of the reported data are based on three repetitions.

Oscillatory rheometry

Oscillatory shear tests, with a small amplitude of $\gamma = 0.05$, which ensured that the nanocomposite melts were tested within the linear viscoelastic

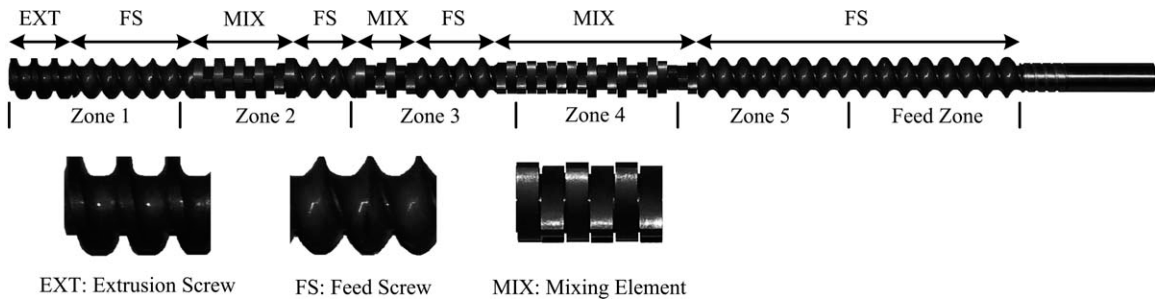

Figure 1 Intermeshing corotating screw profile.

regime, and angular frequencies (ω's), ranging from 100 to 0.016 rad/s, were conducted with a Paar Physica, Graz, Austria MCR500 rheometer in a plate–plate configuration with a 25-mm diameter disc and a gap height of 1 mm.

The tests were performed at 200°C. In each test, the specimen was melted for 5 min; the required gap height was established, and the specimen was equilibrated for 30 min before we measured the various frequencies, starting from the highest frequency. The test specimens were cut from the ends of the injection-molded ISO 3167 multipurpose test specimens. All of the reported data are based on two repetitions.

Uniaxial tensile testing

Uniaxial tensile tests, with a crosshead speed of 50 mm/min, corresponding to a strain rate of 0.01 s^{-1}, were performed on an Instron, Norwood, Massachusetts 5586 tensile testing machine with a 50-kN load cell. Strain measurements at 20°C were performed with an Instron 2630-113 static axial extensometer mounted on the specimen, whereas the measurements at 90°C were performed in an Instron 3119-506 environmental chamber equipped with an Instron 2663-882 video extensometer.

All tests were performed on ISO 3167 multipurpose test specimens, approved for the ISO 527-2 tensile test procedure and measuring 9.9 × 3.75 mm^2 in the cross-sectional dimensions. The reported tensile strength was defined as the yield point on the stress–strain curve, and the tensile modulus reported was the slope of the stress–strain curve up to a 1% strain (secant modulus). All of the reported data are based on five repetitions.

Instrumented Izod impact testing

Instrumented unnotched Izod impact tests were performed on an Instron CEAST 9050 impact tester equipped with a DAS 8000 Junior data-acquisition system, with a sample frequency 1000 kHz and a 50-J instrumented Izod pendulum hammer. The specimens were cut from the center piece of the injection-molded ISO 3167 multipurpose test specimens with final dimension of 63.5 × 9.9 × 3.75 mm^3. All of the reported data are based on five repetitions.

The hammer hit the specimen at 3.46 m/s, and a strain gauge attached to the hammer measured the force between the striking face and the specimen simultaneously with time. The time could be converted into a hammer displacement equivalent to the specimen deflection during impact when the deceleration of the hammer caused by the impact was incorporated. By integration of the force–deflection curve, the energy absorbed by the specimen could be determined at any time during the strike. The three main events during impact were the initial contact between hammer and specimen, the peak point on the force–deflection curve defining crack initiation, and finally, the break of the specimen. The energy absorbed from contact to peak was defined as the crack-initiation energy, and the energy from peak to break was defined as the crack-propagation energy.[9,15,16] The total absorbed energy from contact to break was defined as σ_i and was the sum of the crack-initiation energy and the crack-propagation energy. To clean the value for specimen geometry contributions, the energy was multiplied with a calibration factor in the CEAST software and then divided by the cross-sectional area to yield the following definitions of the fracture initiation energy (E_i), fracture propagation energy (E_p), and σ_i:

$$E_i = \frac{U_{\text{Peak}}\phi}{WT} \tag{3}$$

$$E_p = \frac{(U_{\text{Break}} - U_{\text{Peak}})\phi}{WT} \tag{4}$$

$$\sigma_i = \frac{U_{\text{Break}}\phi}{WT} \tag{5}$$

where U_{Peak} is the energy absorbed until maximum force is reached, U_{Break} is the total energy absorbed until break, W is the width of the specimen, and T is the thickness.

RESULTS AND DISCUSSION

DSC

Calorimetry was performed to evaluate the crystallinity and the crystallization process of the matrix PP in the presence of nanoclay fillers. It is well established that organically modified nanoclays can have a nucleating effect on the PP matrix, which leads to a decreased spherulite size.[17,18] Nanoclays can also act as limiting factors in the crystallization process by blocking the crystal growth and causing a lower χ_C.[19] An important point in the evaluation in the crystallinity of a commercial polymer, such as the HP400R homopolymer, is the high degree of nucleating additives already present in the material, which yield a high initial χ_C. The results from the thermal analysis are presented in Table IV.

The data presented in Table IV showed no significant developments in χ_C and T_m for the materials with regard to T_R. When considering the material composition, we observed smaller differences in χ_C, where the clay-filled materials were less crystalline [38.6% (0.3)] than in the two reference materials [39.5% (0.4)]. This decrease in χ_C with the addition of nanoclay was explained by a decrease in the polymer chain mobility induced by the presence of the clay platelets. More significant changes in the

TABLE IV
Thermal Properties

Sample ID	T_m (°C)	T_c (°C)	χ_C (%)
100/0/0–0	170.8 (0.4)	109.4 (0.7)	39.3 (0.3)
100/0/0–1	170.8 (0.8)	110.6 (0.3)	39.5 (1.2)
100/0/0–2	170.5 (0.9)	111.6 (0.3)	40.0 (0.7)
100/0/0–3	170.5 (1.1)	111.0 (0.1)	39.6 (0.4)
100/0/0–5	170.7 (0.3)	111.5 (0.3)	39.7 (0.1)
96/4/0–1	170.3 (0.7)	115.5 (0.6)	38.4 (0.2)
96/4/0–2	170.9 (0.2)	115.3 (0.4)	38.2 (0.3)
96/4/0–3	170.4 (0.4)	115.2 (0.4)	38.8 (0.3)
96/4/0–5	170.0 (0.7)	115.4 (0.2)	38.9 (0.5)
98/0/2–1	170.3 (0.6)	111.1 (0.2)	39.1 (0.5)
98/0/2–2	170.8 (1.2)	111.4 (0.5)	39.3 (0.9)
98/0/2–3	171.1 (0.3)	111.9 (0.3)	39.2 (0.1)
98/0/2–5	170.0 (0.9)	112.8 (0.3)	40.3 (0.7)
94/4/2–1	169.6 (0.7)	112.1 (0.2)	38.9 (0.5)
94/4/2–2	169.3 (0.5)	112.9 (0.5)	38.1 (0.2)
94/4/2–3	169.9 (0.7)	112.3 (0.1)	38.8 (0.4)
94/4/2–5	69.8 (0.7)	112.7 (0.1)	38.7 (0.8)

The standard deviations are in parentheses.

thermal response were seen with T_c [Fig. 2 and Table IV].

T_c indicates how the crystallization process is initiated during cooling of materials. The initiation of the crystallization process at higher temperatures indicated that a higher number of crystallite nuclei were present or that the polymer chain mobility was higher; this enabled them to move faster to the crystallization area. The material with 4% clay and no compatibilizer had a significantly higher T_c than neat PP (see Fig. 2); this indicated that the clay worked as nuclei for the crystallite growth and probably caused a reduced spherulite size. Upon the addition of PP-*g*-MA, the effect of the clay was reduced; this might have been caused by the presence of PP-*g*-MA in the matrix/clay interface, which reduced the nucleating effect. There was no effect of T_R on T_c of the clay-filled materials. Neat PP showed an increase in T_c between 0 and 60 s of T_R; this might have been due to the increased chain mobility caused by processing-induced material degradation and following the reduced molecular weight.

Oscillatory rheometry

Observations of a nanocomposite in small-strain oscillatory shear revealed a transition from the conventional liquidlike behavior to the so-called pseudo-solidlike behavior (see, e.g., ref. 20). This phenomenon is indicated by a low-frequency plateau in the storage modulus, or in terms of the complex viscosity ($|\eta^*|$), the Newtonian plateau (η_0) observed at low frequencies is replaced by an ever-increasing viscosity at low frequencies. This indicates a yield stress usually associated with soft solids. This low-frequency behavior has been successfully applied as an indicator of the state of particle dispersion in clay-filled polymers.[10,21,22]

To quantify this phenomenon, in ref. 10, the use of a modified Carreau–Yasuda model, introducing a yield stress, was proposed for modeling $|\eta^*|$:

$$|\eta^*| = \frac{\sigma_0}{\omega} + \eta_0[1 + (\lambda\omega)^a]^{\frac{n-1}{a}} \quad (6)$$

where σ_0 is the melt yield stress, η_0 is the zero-shear viscosity, λ is the time constant, a is the Yasuda parameter, and n is the dimensionless power law index. The melt yield stress was used in this study as a direct indicator of the global particle dispersion in the investigated PP-based materials. *Dispersion* in this context is defined as the interconnected process of breaking up aggregates and exfoliating individual clay platelets.

Data were collected for all materials listed earlier, and they mostly showed good reproducibility; that is, the standard deviation was less than 6% of the mean value. The data were fitted to the model described by eq. (6) with the simplex method, as implemented in R, an open-source statistical program. As σ_0 and η_0 both moved the fit up and down, the fitting procedure became unstable for the PNC materials because of their yield stress. To ensure a consistent behavior of σ_0, we adopted a strategy of fitting the materials compounded only once first ($n = 1$), as the data from these did not have a pronounced yield stress, and then keeping the value of η_0 constant for the rest of the data. The obtained fitting parameters for the different materials are listed in Table V, and the resulting models are plotted in Figure 3, together with the measured $|\eta^*|$.

The R^2 values indicated that the model had the ability to describe the collected data; the behavior of the nanocomposites was particularly well described in the whole frequency range [Fig. 3(c,d)], whereas

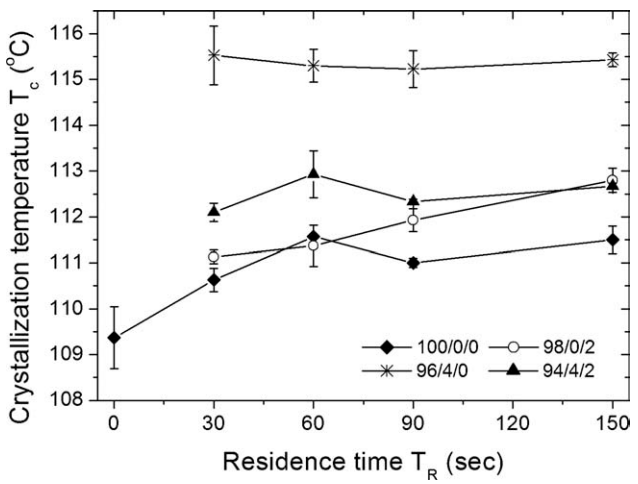

Figure 2 T_c as a function of T_R.

TABLE V
Fitted Parameters for the Carreau–Yasuda Model [eq. (6)]

Sample ID	σ_0	λ	a	n	η_0	R^2
100/0/0–0	NA	0.150	1.532	0.682	635.31	0.981
100/0/0–1	NA	0.145	1.649	0.695	592.13	0.972
100/0/0–2	NA	0.136	1.687	0.702	530.19	0.971
100/0/0–3	NA	0.135	1.764	0.704	506.45	0.965
100/0/0–5	NA	0.113	1.912	0.724	391.02	0.954
96/4/0–1	0[a]	0.132	1.075	0.624	832.1	0.987
96/4/0–2	3.567	0.205	1.860	0.688	—	0.986
96/4/0–3	8.639	0.216	2.076	0.697	—	0.985
96/4/0–5	12.042	0.195	1.264	0.678	767.22[b]	0.997
98/0/2–1	NA	0.147	1.632	0.691	600.75	0.974
98/0/2–2	NA	0.147	1.778	0.697	558.45	0.965
98/0/2–3	NA	0.139	1.693	0.696	542.71	0.971
98/0/2–5	NA	0.122	1.885	0.722	404.25	0.956
94/4/2–1	0.419	0.088	0.851	0.563	806.74	0.9997
94/4/2–2	18.104	0.261	1.892	0.711	—	0.993
94/4/2–3	45.027	0.294	3.126	0.723	—	0.988
94/4/2–5	54.747	0.432	1.294	0.717	—	0.995

NA, not applicable.
[a] Negative σ_0 = =1.0114984, probably due to degradation.
[b] Pronounced effect of degradation of the matrix material.

the degradation behavior of the unfilled reference systems at low frequencies was not fully described by the model [Fig. 3(a,b)].

For the reference materials, neat PP and PP with PP-*g*-MA [Fig. 3(a,b)], the level of η_0 decreased monotonically with the number of extrusion cycles and, hence, T_R. As η_0 was proportional to the molecular weight, this merely indicated the thermal and mechanical degradation of the material. This degradation was expected and has previously been shown to occur during the extrusion of PP and to result in a reduction in the molecular weight.[23] The rate of degradation with regard to T_R was constant and comparable for both reference materials [see Fig. 4].

The prepared composites, PP with OMMT [Fig. 3(c)] and PP with OMMT and PP-*g*-MA [Fig. 3(d)], exhibited no real η_0, except for the materials extruded once. For these two composites, the $|\eta^*|$, at the lowest frequency increased monotonically with the number of extrusion cycles and, hence, T_R [see Fig. 5]; this indicated better dispersed OMMT throughout the PP matrix.

It is clear from Figure 5 that the melt yield stress increased significantly faster for the composite containing PP-*g*-MA than for the one without. This was explained by the ability of the compatibilizer to facilitate exfoliation of the OMMT in the PP matrix and, consequently, to obtain a higher degree of dispersion, as measured by oscillatory rheometry.

Besides the changed behavior at low frequencies, $|\eta^*|$ was approximately 30% higher for the filled materials than for the unfilled materials; this was associated with the addition of filler to the matrix.

For the PP with OMMT and the PP with OMMT and PP-*g*-MA only, the materials extruded five times had indications of thermal and mechanical degradation; this indicated that the formation of a soft solid masked the effect of the thermal and mechanical loads to a certain degree.

Tensile properties

A uniaxial tensile test was performed to evaluate the small-strain mechanical properties at low deformation rates, with regard to both increased T_R and blend composition. The tests were performed at ambient and elevated temperatures, and the results are presented in Figure 6 with regard to T_R. The data showed good reproducibility for tensile strength with standard deviations within 2% of the mean values. The modulus was less consistent, especially at ambient temperature, with standard deviations of 5–15% of the average [Fig. 6(b)]. For the moduli at elevated temperatures, the deviation was typically within 5% of the mean.

Neat PP and PP with PP-*g*-MA, shown in Figure 6(a–d), showed no sign of any reductions in the tensile strength and tensile modulus at ambient or elevated temperatures with regard to increased T_R and after degradation. This correlated with earlier findings[24,25] in the investigation of the effect of the processing-induced degradation of PP on the mechanical properties. They concluded that small-strain properties, such as the tensile strength, modulus, and σ_i, are only slightly affected, despite the PP chain scission and reduced molecular weight. Increased crystallinity was given as the explanation for the preserved small-

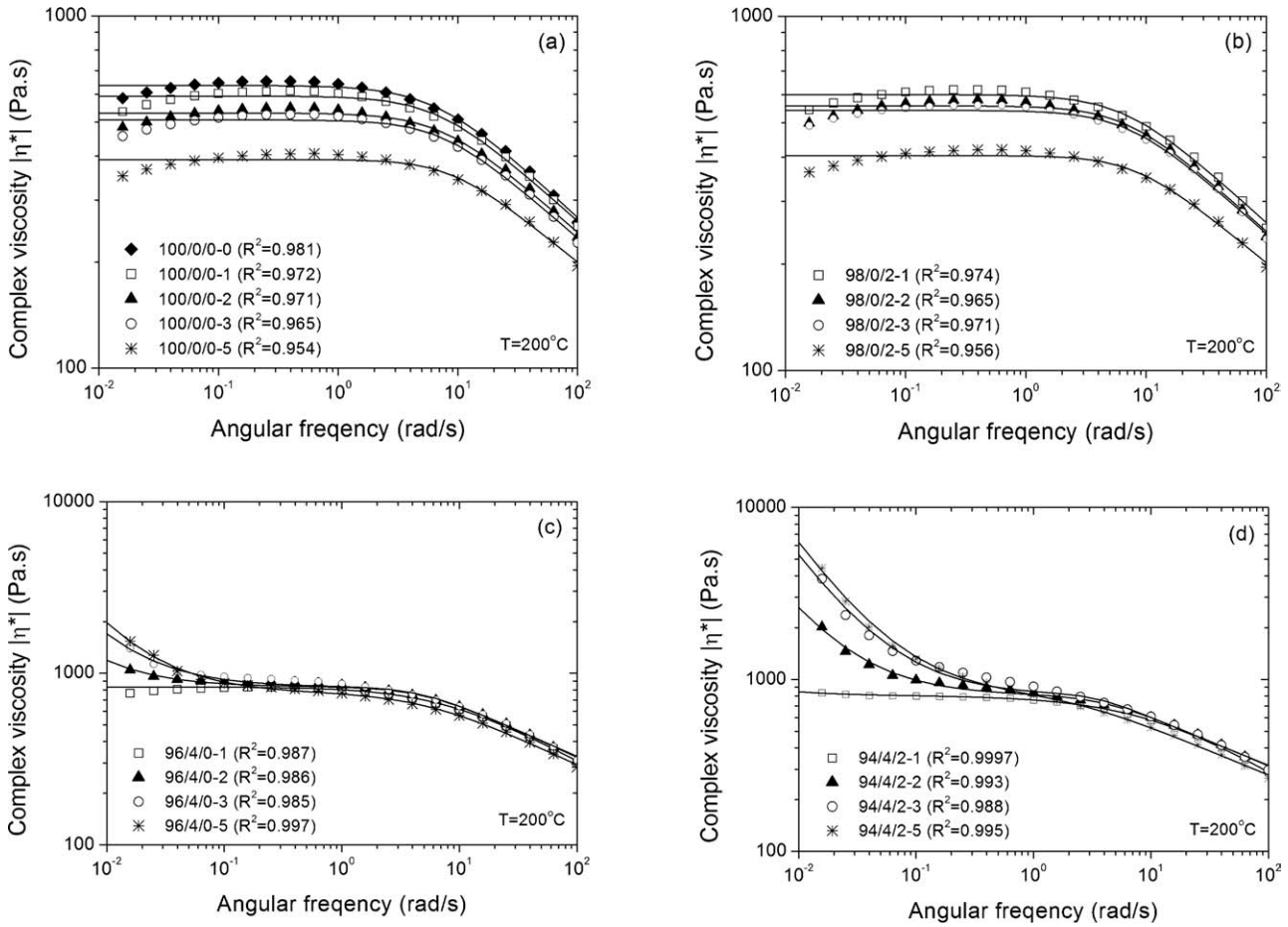

Figure 3 $|\eta^*|$ fitted to the modified Carreau–Yasuda model [eq. (6)]: (a) neat PP, (b) PP with PP-*g*-MA, (c) PP with OMMT, and (d) PP with OMMT and PP-*g*-MA.

strain mechanical response originating from the increased chain mobility due to reduced molecular weight. With regard to the thermal data presented in Table IV, it was not possible to show any increase in the crystallinity for neat PP and PP with PP-*g*-MA with regard to T_R. Instead, the crystallinity was maintained; this correlated well with the fact that no effects of T_R on the tensile strength and tensile modulus on the reference materials were observed. The initial variation of neat PP tensile strength at 20°C with regard to T_R [see

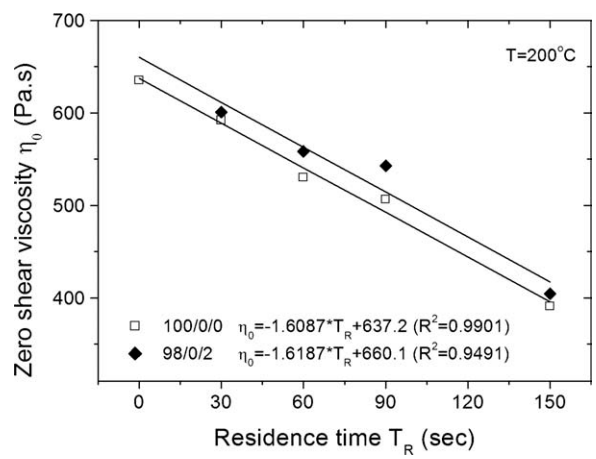

Figure 4 Zero-shear viscosity for the two unfilled reference materials with regard to T_R, showing the rate of degradation.

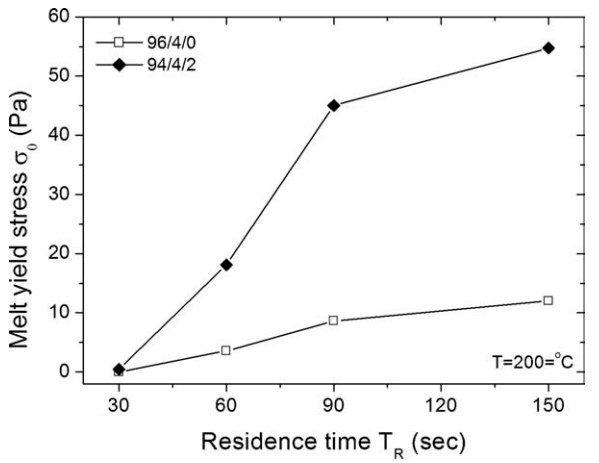

Figure 5 Melt yield stress for the two nanocomposites with regard to T_R, indicating improved dispersion of the clay platelets.

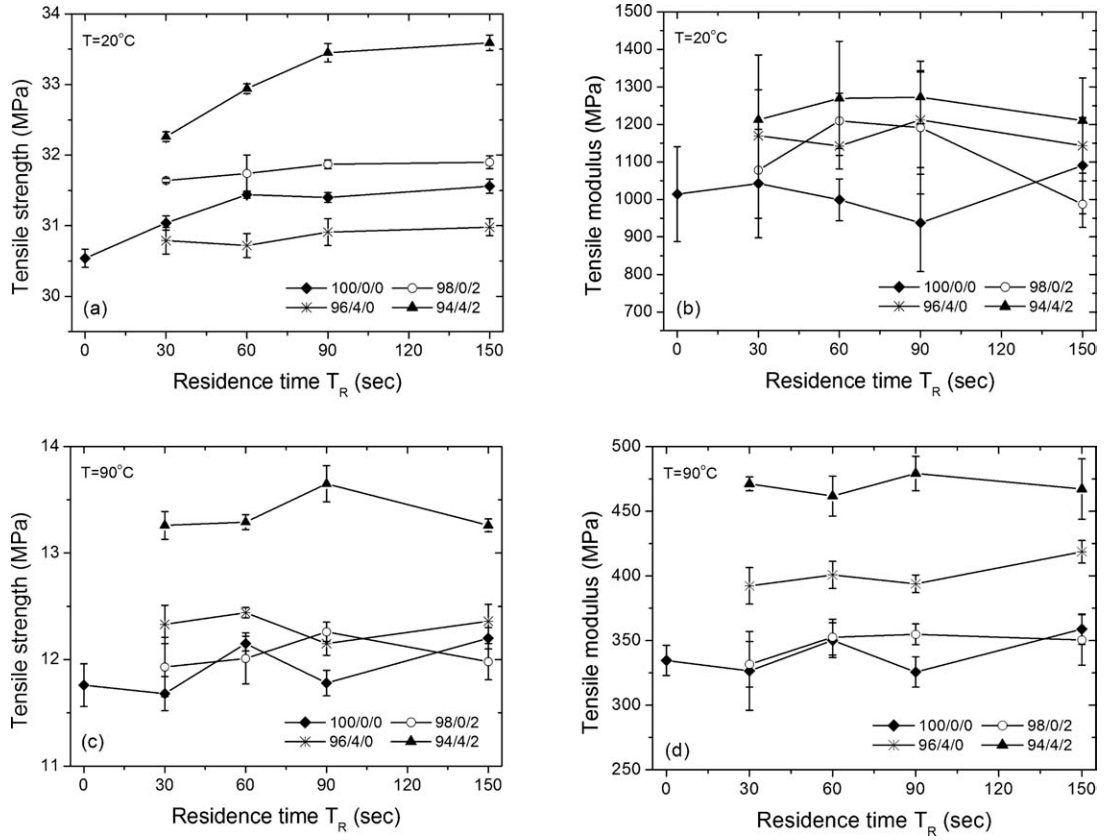

Figure 6 Small-strain mechanical properties: (a) tensile strength at 20°C, (b) tensile modulus at 20°C, (c) tensile strength at 90°C, and (c) tensile modulus at 90°C.

Fig. 6(a)] might have been connected to the differences in T_c shown in Figure 2.

The tensile strength and tensile modulus of the two nanocomposites were, with one minor exception, similarly unaffected by the increased T_R and followed increased dispersion at both ambient and elevated temperatures, as shown in Figure 6(a–d). The only exception was that the tensile strength of the composite containing OMMT and PP-*g*-MA measured at 20°C increased slightly with increasing T_R. No changes were found in χ_C, as presented in Table IV, so the small increase was attributed to the improved dispersion of the clay filler, which enabled a slight increase in the reinforcing effect.

On the basis of the obtained data, no significant effects of increased T_R and following dispersion could be found on the small-strain tensile mechanical properties. In Table VI, the tensile properties for the four materials are reported as averages, regardless of the applied T_R.

The primary changes in the tensile strength were a 6% increase from neat PP to PP with OMMT and PP-*g*-MA at 20°C and a 12% increase at 90°C. The effect of adding only OMMT without compatibilizer was insignificant on the tensile strength, as was the effect of adding compatibilizer without any OMMT. The tensile modulus of PP increased by 22% at 20°C and by 38% at 90°C with the addition of OMMT together with the PP-*g*-MA compatibilizer. In summary, the addition of OMMT together with the used PP-*g*-MA compatibilizer was shown to have a reinforcing effect on the PP matrix

TABLE VI
Average Tensile Properties Regardless of T_R

Sample ID	Tensile strength 20°C (MPa)	Tensile modulus 20°C (MPa)	Tensile strength at 90°C (MPa)	Tensile modulus at 90°C (MPa)
100/0/0	31.2 (0.4)	1017 (121)	11.9 (0.3)	339 (21)
96/4/0	30.9 (0.2)	1167 (97)	12.3 (0.2)	401 (14)
98/0/2	31.8 (0.2)	1116 (144)	12.1 (0.2)	347 (17)
94/4/2	33.1 (0.5)	1241 (126)	13.4 (0.2)	470 (16)

The standard deviations are in parentheses.

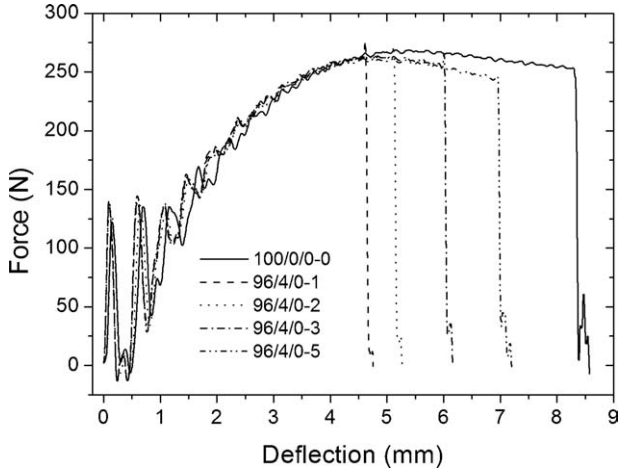

Figure 7 Force–deflection curves for the nanocomposites with PP and OMMT extruded 1, 2, 3, and 5 times, together with unextruded neat PP.

material, which was more pronounced at elevated temperatures.

Impact properties

The impact properties of the materials with regard to increased T_R were investigated by instrumented unnotched Izod impact tests, which gave detailed information about the impact behavior. On the basis of the conclusions from the rheological measurements, these tests made it possible to relate the impact behavior with the degree of nanofiller dispersion through T_R. Impact curves for the two nanocomposites subjected to a varying number of extrusion cycles, together with the response of neat PP, are shown in Figure 7 for PP with OMMT and in Figure 8 for PP with OMMT and PP-*g*-MA.

As described previously, σ_i could be divided into E_i from contact until the curve peak and into E_p from the peak until the breaking of the specimen. The first part of all of the curves consisted of two initial peaks related to inertial effects related to the first contact between the hammer and the specimen. In general, small differences were observed in the crack-initiation phase, although a reinforcing effect in the nanocomposite containing OMMT and PP-*g*-MA was observed. Besides this, there was a tendency toward deflection at peak increases when the extrusion cycles were repeated, and T_R and dispersion increased. The resulting E_i, together with σ_i and E_p, are presented in Table VII, where it can be seen that E_i for the reference materials was constant, whereas it increased slightly for both investigated composites with the number of repeated extrusion cycles and T_R.

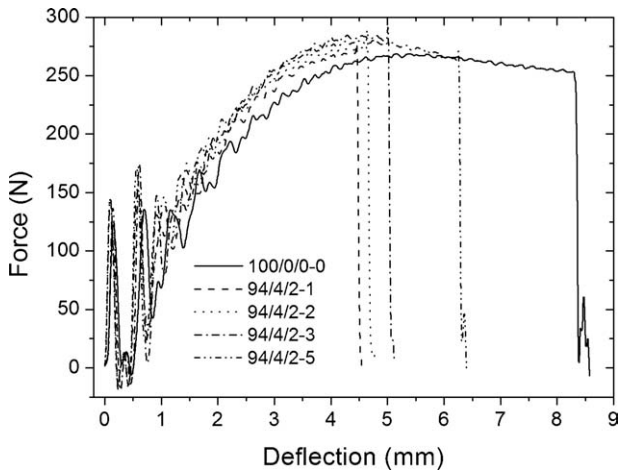

Figure 8 Force–deflection curves for the nanocomposites with PP, OMMT, and PP-*g*-MA extruded 1, 2, 3, and 5 times, together with unextruded neat PP.

TABLE VII
Impact Properties

Sample ID	E_i (kJ/m^2)	E_p (kJ/m^2)	σ_i (kJ/m^2)
100/0/0–0	26.5 (0.0)	20.2 (2.5)	46.7 (2.5)
100/0/0–1	26.6 (0.1)	19.8 (2.2)	46.4 (2.2)
100/0/0–2	26.4 (0.1)	22.2 (0.9)	48.6 (1.0)
100/0/0–3	26.2 (0.2)	21.3 (0.6)	47.5 (0.5)
100/0/0–5	26.3 (0.2)	20.4 (1.3)	46.7 (1.3)
96/4/0–1	21.6 (0.7)	0.6 (0.5)	22.2 (1.1)
96/4/0–2	22.8 (0.2)	2.8 (0.6)	25.6 (0.6)
96/4/0–3	23.5 (0.1)	8.3 (2.9)	31.9 (3.0)
96/4/0–5	23.9 (0.2)	14.5 (3.7)	38.5 (3.6)
98/0/2–1	25.9 (0.3)	20.1 (0.6)	46.0 (0.6)
98/0/2–2	26.0 (0.2)	20.9 (0.7)	46.9 (0.8)
98/0/2–3	26.1 (0.2)	20.3 (0.7)	46.4 (0.9)
98/0/2–5	26.2 (0.2)	19.7 (0.7)	45.8 (0.9)
94/4/2–1	21.3 (0.7)	0.6 (0.2)	21.9 (0.9)
94/4/2–2	22.0 (0.6)	1.9 (1.3)	23.9 (1.8)
94/4/2–3	23.0 (0.6)	4.6 (1.9)	27.6 (2.6)
94/4/2–5	23.4 (0.1)	14.4 (1.8)	37.9 (1.7)

The standard deviations are in parentheses.

Beyond the peak force and the initial crack formation, the changes between the unfilled and filled materials became more significant, and the effects of T_R and, hence, dispersion played important roles. In general, the deflection at break decreases when fillers are introduced into the system, regardless of the addition of compatibilizer, as shown in Figures 7 and 8. With an increase in T_R and, through that, an increase in the particle dispersion, the deflection at break significantly increased for both nanocomposites, as shown in Table VII.

Because of the large effect of increased dispersion on the deflection at break and following E_p, this was closely related to the changes in σ_i of the materials. σ_i with regard to T_R is shown in Figure 9, where a monotonic increase with T_R is clear.

The increase in σ_i from least to best filler dispersion was on the order of 70% from approximately 22 to 38 kJ/m^2 for both composite materials. The composite exposed to the longest T_R still resulted in an

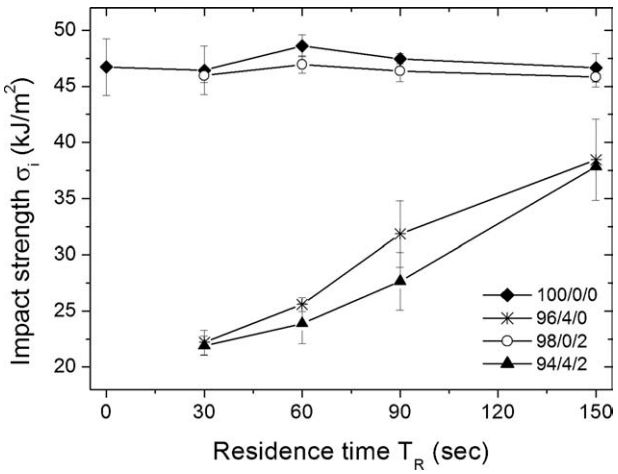

Figure 9 Unnotched Izod σ_i with regard to T_R.

σ_i 20% below that of the reference materials, neat PP and PP with PP-*g*-MA. The reference materials showed no sign of degradation in their impact properties with increased T_R, as shown in Table VII and Figure 9. This followed the conclusions from refs. 24 and 25 that small-strain mechanical properties are only moderately affected by material degradation.

The primary parameter affecting the impact behavior of the investigated composites with regard to increased T_R and particle dispersion was the deflection at break, which led to increased E_p; this corresponded to approximately 80% of the improvements of the nanocomposite σ_i [see Fig. 10]. The increased E_p was most likely caused by reductions in the number and size of clay aggregates working as stress concentrators and facilitating the propagation of the crack across the specimen.

The remaining 20% of the improvement in σ_i, from least to best dispersed nanocomposites, originated from the increased peak force and deflection at peak, which led to an increased E_i. The increased peak force was due to the reinforcing effect of the nanoparticles, which was only seen with the use of PP-*g*-MA, and the increased deflection was probably due to a reduction in sites for crack initiation after the increased dispersion with T_R.

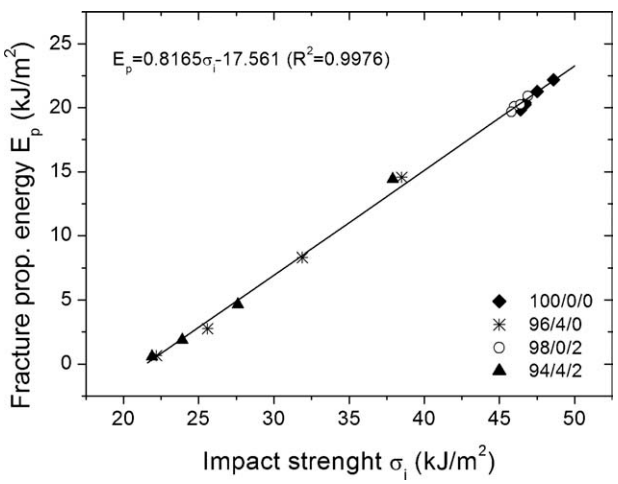

Figure 10 E_p with regard to σ_i.

CONCLUSIONS

Two nanocomposites and two reference materials were prepared by TSE, and T_R gradually increased when the extrusion cycle was repeated multiple times to produce nanocomposites with different dispersion states. It was found that proper particle dispersion was a major factor to control in obtaining acceptable impact properties and that smaller improvements in the crack initiation could be completely masked by a large decrease in E_p. The following conclusions were drawn:

1. Oscillatory rheometry showed a monotonic decrease in the zero-shear viscosity of the reference materials with regard to T_R, which is proportional to a reduction in average molecular weight.
2. The melt yield stress, as defined in the modified Carreau–Yasuda model, increased monotonically with T_R for the nanocomposites, and this indicated improved particle dispersion.
3. The small-strain tensile mechanical properties were generally unaffected by increased T_R for both the nanocomposites and reference materials.
4. The nanocomposite σ_i increased monotonically with increased T_R by approximately 70% from the worst to best dispersed state but was still 20% below the level for neat PP.
5. The increased σ_i was mainly due to increased E_p and less to E_i. The propagation energy contributed to approximately 80% of the increase in σ_i, whereas the energy to initiate crack formation accounted for 20% of the increase.

References

1. Chinellato, A. C.; Vidotti, S. E.; Hu, G. H.; Pessan, L. A. Compos Sci Technol 2010, 70, 458.
2. Lee, Y. H.; Park, C. B.; Sain, M.; Kontopoulou, M.; Zheng, W. J Appl Polym Sci 2007, 105, 1993.
3. Qin, H. L.; Zhang, S. M.; Zhao, C. G.; Feng, M.; Yang, M. S.; Shu, Z. J.; Yang, S. S. Polym Degrad Stab 2004, 85, 807.
4. Yuan, Q.; Misra, R. D. K. Polymer 2006, 47, 4421.
5. Alkbari, B.; Bagheri, R. J Appl Polym Sci 2009, 114, 3751.
6. Deenadayalan, E.; Vidhate, S.; Lele, A. Polym Int 2006, 55, 1270.
7. Li, P.; Song, G.; Yin, L.; Wang, L.; Ma, G. J Appl Polym Sci 2008, 108, 2116.
8. Chen, B.; Evans, J. R. G. Soft Matter 2009, 5, 3572.
9. Rattanawijan, W.; Amornsakchai, T.; Amornsakchai, P.; Petiraksakul, P. J Appl Polym Sci 2009, 113, 1887.

10. Lertwilmolnun, W.; Vergnes, B. Polymer 2005, 46, 3462.
11. Lertwimolnun, W.; Vergnes, B. Polym Eng Sci 2007, 47, 2100.
12. Li, J.; Ton-That, M.; Leelapornpisit, W.; Utracki, L. A. Polym Eng Sci 2007, 47, 1447.
13. Zhu, L. J.; Xanthos, M. J Appl Polym Sci 2004, 93, 1891.
14. van Krevelen, D. W. Properties of Polymers; Elsevier: Amsterdam, 2003; Chapter 5, p 120.
15. Hristov, V. N.; Lach, R.; Grellmann, W. Polym Test 2004, 23, 581.
16. Kargerkocsis, J. Compos Sci Technol 1993, 48, 273.
17. Ahangari, M. G.; Fereidoon, A.; Kordani, N.; Garmabi, H. Polym Bull 2011, 66, 239.
18. Perrin-Sarazin, F.; Ton-That, M.; Bureau, M.; Denault, J. Polymer 2005, 46, 11624.
19. Ma, J.; Zhang, S.; Qi, Z.; Li, G.; Hu, Y. J Appl Polym Sci 2002, 83, 1978.
20. Drozdov, A. D.; Jensen, E. A.; Christiansen, J. d. C. Int J Eng Sci 2008, 46, 87.
21. Wang, Y.; Chen, F. B.; Wu, K. C.; Wang, J. C. Polym Eng Sci 2006, 46, 289.
22. Marchant, D.; Jayaraman, K. Ind Eng Chem Res 2002, 41, 6402.
23. Canevarolo, S. V.; Babetto, A. C. Adv Polym Technol 2002, 21, 243.
24. da Costa, H. M.; Ramos, V. D.; de Oliveira, M. G. Polym Test 2007, 26, 676.
25. GuerricaEchevarria, G.; Eguiazabal, J. I.; Nazabal, J. Polym Degrad Stab 1996, 53, 1.